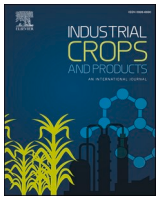
Industrial Crops & Products 252 (2026) 124404



Contents lists available at ScienceDirect

Industrial Crops & Products

journal homepage: www.elsevier.com/locate/indcrop





Mechano-assisted synthesis of lignin-based hybrid materials for antimicrobial applications

Marianna Vescovi [a], Diego Pini [a], Andrea Gustinelli [b], Giorgia Bignami [b], Andrea Migliori [c], Lisa Menegaldo [d], Francesca Bonvicini [d], Dominga Rogolino [a,*,1], Paolo Pelagatti [a,*,1]

[a] Department of Chemistry, Life Sciences and Environmental Sustainability, University of Parma, Parma, 43124, Italy
[b] Department of Veterinary Medical Sciences (DIMEVET), Alma Mater Studiorum University of Bologna, Via Tolara Di Sopra, 50, Ozzano Dell'Emilia, Bologna, 40064, Italy
[c] CNR-ISMN Sezione di Bologna, via Gobetti 101, Bologna, 40129, Italy
[d] Department of Pharmacy and Biotechnology, University of Bologna, Via Massarenti 9, Bologna, 40138, Italy

ARTICLE INFO

Keywords:
Lignin
Hybrid materials
Mechanochemistry
Cuprite
Zincite
Antimicrobial activity

ABSTRACT

Lignin and lignin-based materials represent a great opportunity to develop novel materials that combine the antioxidant and antibacterial properties of the polyphenolic matrix with the biological profile of an inorganic phase. We here use a mechano-assisted approach to obtain straightforward isolation of the hybrid materials HMW@ZnO, HMW@Cu_2O, and the mixed-oxide HMW@ZnO_Cu_2O, where HMW (High Molecular Weight) is a Kraft lignin from *Pinus taeda*. Full material characterization confirmed that mechano-synthesis is an efficient method for smoothly forming products with controlled amounts of Zn, Cu or both, embedded within the Kraft lignin matrix. *In vitro* testing against four pathogens (*Staphylococcus aureus*, *Lactococcus garvieae*, *Escherichia coli*, and *Aeromonas veronii*) showed that all lignin hybrids exhibited enhanced antimicrobial activity compared to pure reference metal oxides. Crucially, the HMW@ZnO_Cu_2O hybrid demonstrated superior efficacy (lower MBC values) against *S. aureus* and *A. veronii* compared to the single-oxide hybrids, suggesting a positive interaction mechanism between the combined metal phases. These findings validate mechano-assisted synthesis as an effective route for developing potent, lignin-based antimicrobials.

1. Introduction

Mechanochemistry has emerged as a sustainable and efficient synthetic approach, since it offers the possibility to induce chemical transformations by mechanical energy, (Boldyrev and Tkáčová, 2000) avoiding the use of solvents (Wenger and Hanusa, 2023). It aligns with green chemistry principles, providing waste reduction, energy efficiency, and simplified reaction setups, (Chetry, 2025) finding applications across diverse fields, from organic and inorganic chemistry to material science, including nanotechnology (James et al., 2012). This work investigates the potential of a mechano-assisted approach as a sustainable synthetic route for preparing hybrid materials that integrate metal oxides within an amorphous lignin matrix for antibacterial applications. Lignin is a natural, abundant, and biodegradable biopolymer, endowed of antioxidant and antimicrobial properties (Lu et al., 2022; Vasile and Baican, 2023). Its antimicrobial features are well-established, since it is known to inhibit the growth of various microorganisms, including *Escherichia coli*, *Staphylococcus aureus*, *Pseudomonas aeruginosa*, *Klebsiella pneumoniae*, and *Candida albicans* (Karmanova et al., 2021; Dong et al., 2011). These effects are attributed to the polyphenolic structure of lignin, which damages cell membranes and causes cellular lysis (Beisl et al., 2017). Currently, most technical lignins are burnt to produce steam and energy and they are typically considered a waste product in paper pulp and biorefinery industry. Research is increasingly focusing on lignin high-value applications, including its use in producing resins, additives, plastics, films, and fibres (Yu et al., 2023). There is also significant interest in its catalytic degradation into valuable aromatic monomers (Radhika et al., 2022) and its potential as a biosorbent for heavy metal pollutant removal (Vescovi et al., 2023; Huang et al., 2026). Lignin has also been used for the encapsulation and controlled release of bioactive molecules, as antimicrobials or for anti-tumor applications (Verdini et al., 2022; Wang et al., 2025, 2024).

* Corresponding authors.
E-mail addresses: dominga.rogolino@unipr.it (D. Rogolino), paolo.pelagatti@unipr.it (P. Pelagatti).
[1] Authors equally contributed to the work.

https://doi.org/10.1016/j.indcrop.2026.124404
Received 23 February 2026; Received in revised form 23 August 2026; Accepted 15 September 2026
0926-6690/© 2026 The Authors. Published by Elsevier B.V. This is an open access article under the CC BY-NC-ND license (http://creativecommons.org/licenses/by-nc-nd/4.0/).

The combination of lignin with metal oxides endowed with antimicrobial properties, such as zinc oxide and copper(I) oxide, could provide the opportunity to achieve synergistic effects, potentially at low metal concentration, as demonstrated by previous works of our research group (Vescovi et al., 2025; Gazzurelli et al., 2022, 2020). Preparing these antimicrobial hybrid materials via a mechano-assisted approach could pave the way for sustainable practical applications in agriculture and zootechnics. In the realm of sustainable technologies, the mechanochemical approach has emerged as a distinctive and effective method to produce metal-oxide nanoparticles (NPs), (Tsuzuki, 2021; Klapiszewska et al., 2021) materials that have become fundamental in various fields, including electronics, biomedicine, pharmaceutics and agriculture (Tsuzuki, 2009). ZnO, in particular, has diverse applications spanning from photocatalysis, use in electronic devices, antibacterial effects and as source for zinc micronutrient in agrochemical or zootechnical field (Sharma et al., 2022). Some strategies for the preparation of ZnO nanoparticles *via* mechanochemistry have already been explored in the literature. For instance, Salah et al. (Salah et al., 2017) used a high-energy ball mill to comminute commercial microcrystalline ZnO powder, producing nearly spherical NPs with uniform sizes and inducing structural changes, including lattice relaxation and deep-level defects. These modifications are believed to strengthen the antibacterial potential of ZnO NPs, as the increased surface area should enhance the generation of reactive oxygen species (ROS), effective for bacterial growth inhibition (Abebe et al., 2020). Tòthová et al (Tothova et al., 2020). employed a two-step process based on the initial synthesis of phase-pure hydrozincite ($Zn_5(CO_3)_2(OH)_6$), followed by heating to produce ZnO NPs with high surface area. Similarly, Ao et al. (Ao et al., 2006) synthesized ZnO nanocrystals using a two-step method, demonstrating that milling time can directly influence the final crystal size. Furthermore, copper compounds have long been used as effective plant protection agents, although concerns over copper environmental impact have been raised. Cu-containing hybrid materials with lower environmental footprint have been developed in our laboratory, also under mechanochemical conditions, combining lignin with copper compounds such as brochantite, $Cu_4(OH)_6(SO_4)$, and cuprite, Cu_2O, the last obtained *in situ* by lignin induced Cu(II) reduction (Gazzurelli et al., 2022, 2020). In particular, lignin@Cu_2O is effective against *Listeria monocytogenes* and *Rhizoctonia solani* at low copper dosage, as evidenced by *in vitro* and *in vivo* tests conducted on tomato plants. Potential mechanisms about Cu(I) effectiveness were hypothesized by Meghana et al., which supposed that cuprous oxide generates hydroxyl radicals, which can cause cellular damage through Fenton reactions (Meghana et al., 2015). Despite the known antibacterial properties of cuprite, (Jacukowicz-Sobala et al., 2023; Lejeune et al., 2023) to the best of our knowledge, there are few reports on its mechano-assisted synthesis (Khayati et al., 2013). Based on these considerations, we focused on the one-pot mechano-assisted synthesis of hybrid materials of the type HMW@ZnO, HMW@Cu_2O and HMW@ZnO_Cu_2O, featured by different contents of the two metals, where HMW (High Molecular Weight) is a Kraft lignin from *Pinus taeda*. The material can be described as a hybrid nanocomposite, comprising two distinct components: the polymeric matrix and the crystalline phases, likely interacting by weak non covalent interactions. The full material characterization has been achieved by the combination of a series of techniques aimed at characterizing both the biopolymeric matrix and the inorganic phases formed, trying to unveil the parameters that affect the crystallization of the inorganic oxides NPs. In fact, lignin can act as capping agent during the crystallization of the oxide NPs exerting a control on the dimension of the final crystals. We also investigated the possibility of simultaneously incorporating the two distinct inorganic phases. The results confirmed that lignin can effectively function as a biopolymeric host for the crystallization of the metal oxides. By optimizing the synthetic parameters, we successfully tuned the relative concentrations of the two oxides into the final material, enabling the development of a heterometallic hybrid system where the cooperative effect of the copper and zinc phases are expected to amplify the antimicrobial efficacy via complementary mechanisms of action (Hassan et al., 2017). There is a general consensus on the enhanced antimicrobial activity observed with NP-materials containing Cu_2O and ZnO (Fen et al., 2025; Li et al., 2022; Abebe et al., 2020) but, to the best of our knowledge, there are not reports dealing with lignin-based materials containing both oxides. The isolated materials will be hereinafter labelled by specifying the weight percent of metal present in the material, accordingly to ICP-AES data: HMW@ZnO_X% (X = 5, 13%), HMW@Cu_2O_Y% (Y = 4, 14%) and HMW@ZnO_Cu_2O_X% (X = 7%). The antimicrobial activity of these metal oxide hybrid materials was evaluated *in vitro* against bacterial species of relevance to human health (*Staphylococcus aureus* and *Escherichia coli*) as well as animal and environmental systems (*Lactococcus garvieae* and *Aeromonas veronii*). Antimicrobial resistance is widely documented in major human pathogens such as *Staphylococcus aureus* and *Escherichia coli*, which are key priority organisms under World Health Organization Global Antimicrobial Resistance and Use Surveillance System (WHO GLASS), while WHO also emphasizes a One Health approach that includes resistance monitoring in animal and environmental bacteria relevant to aquaculture systems (World Health Organization, 2014, 2022). In addition, *L. garvieae* and *A. veronii* are gaining importance as fish pathogens in Mediterranean aquaculture (Esposito et al., 2025; Salogni et al., 2024; Zrnčić, 2020), further highlighting the potential of these materials in aquatic pathogen contexts beyond human health applications. Ultimately, this study aims to develop innovative, efficient, and environmentally friendly strategies for fabricating lignin-based hybrid materials, paving the way for their potential use in agrochemical and zootechnical formulations, and offering a viable alternative to conventional synthetic protocols.

2. Experimental part

2.1. Materials and methods

HMW (Biopiva395®, Kraft softwood lignin from *Pinus taeda*, Mw 5950–6000 g/mol, Mn 1560–1565 g/mol) was kindly provided by UPM-Kymmene Oyj (Helsinki, Finland) and Green Innovation GmbH (Innsbruck, Austria). All the reagents were used as received with no further purification. The mechano-assisted syntheses were conducted with a planetary ball mill Retsch® PM100 using a 80 mL agate jar or a 500 mL zirconia jar. Liquid Assisted Grinding (LAG) conditions correspond to η values $\leq$ 2, where η = mL of water/g of solids. Experimental details about materials characterization (PXRD, FT-IR, ICP-AES, SEC, TEM) are reported in the Supporting Information Paragraph.

Four different bacteria were included in the study: the two laboratory strains, *S. aureus* (ATCC 25923) and *E. coli* (ATCC 25922), were obtained from the American Type Culture Collection (ATCC, Manassas, VA, USA). The other two bacteria used, *A. veronii* (ITT 39/25) and *L. garvieae* (ITT 44/25), were obtained from the repository of the Fish Pathology Unit of the Department of Veterinary Medical Sciences of the University of Bologna and had been isolated during mortality outbreaks in Italy. *A. veronii* was isolated from European seabass (*Dicentrarchus labrax*) and *L. garvieae* from gilthead seabream (*Sparus aurata*) farmed in Tuscany during 2025. ATCC strains were routinely grown on blood agar plates purchased by Biolife Italiana S.r.l while *A. veronii* and *L. garvieae* on Tryptic Soy Agar by Oxoid, Thermo Fisher Scientific. For antimicrobial experiments, Mueller–Hinton broth and Standard Count Agar were purchased by CondaLab (Laboratorios Conda S.A., Madrid, Spain).

2.2. Synthesis of the materials

HMW@ZnO_X% (X = 5, 13%) and HMW@Cu_2O_Y% (Y = 4, 14%). In an 80 mL agate jar, HMW, zinc or copper salt and 5 agate spheres (15 mm ø, ~ 4,7 g) were loaded according to the mass ratio reported in Table 1 and Table S1, intended to reach 5% and 10% of metal upload in the final material. A pre-mixing of the reagents was performed for 1 min at 200 rpm. Then, NaOH solution (4 or 5 mol of NaOH with respect to

Table 1
Stoichiometric ratios of reagents for the preparation of HMW@ZnO_X% (X = 5, 13%) and HMW@Cu_2O_Y% (Y=4, 14%), by using $ZnSO_4·7H_2O$ or $CuSO_4·5H_2O$, respectively. M = zinc or copper.

	HMW/MSO_4 (g/g)	NaOH/M molar ratio	η (μL/mg)	M% (ICP data)
HMW@ZnO_5%	7.5/1.8	5/1	1.70	4.7 ± 0.2
HMW@ZnO_13%	6.7/3.4	4/1	0.93	13.1 ± 0.1
HMW@Cu_2O_4%	8.5/1.88	4/1	1.40	3.9 ± 0.1
HMW@Cu_2O_14%	6.9/3.5	4/1	1.06	14.3 ± 0.1

metal) was added. The concentration of the solution was varied accordingly to the amount of reagent to reach LAG conditions (η ≤ 2, Table 1). The mixture was then ground at 300 rpm for 30 min. The reported grinding times and rotational speeds reflect the optimized parameters required to achieve full conversion of the starting materials. The brown product obtained was dried in a heating chamber at 95 °C overnight. The obtained powder was washed with distilled water (25 mL per gram), centrifuged (300 rpm for 5 min) and dried again at 95 °C overnight. All the experiments were performed at least in duplicate. The amount of metal effectively uploaded was determined by ICP-AES (see Table 1). No contamination of silica has been detected, as inferred by EDX analyses reported in the Supporting Information paragraph.

For the Zn-containing materials a scale up to 60 g of final materials was also optimized; the experimental details are reported in the Supporting Information as Procedure S1 (see also Table S2).

HMW@ZnO_Cu_2O_7%: In a 80 mL agate jar, HMW (6.8 g), $ZnSO_4·7H_2O$ (3.4 g), $CuSO_4·5H_2O$ (2.9 g), corresponding to a NaOH/Zn^{2+}/Cu^{2+} molar ratio of 6/1/1 and 5 agate spheres (1 5 mm ø, ~4,7 g) were loaded. A pre-mixing of the reagents was performed for 1 min at 200 rpm. Then, a NaOH aqueous solution was added (0.070 mol, 7 M). The concentration of the solution was chosen to reach LAG conditions (η = 0.8). The mixture was ground at 300 rpm for 30 min. The reported grinding times and rotational speeds reflect the optimized parameters required to achieve full conversion of the starting materials. The brown product obtained was dried in the heating chamber at 95 °C overnight. The powder was washed with distilled water (25 mL per gram), centrifuged (300 rpm for 5 min) and dried again at 95°C overnight. All the experiments were performed at least in duplicate. The amount of metals uploaded was determined by ICP-AES (Cu% mean ± SD: 7.35 ± 0.06; Zn% mean ± SD: 7.10 ± 0.09). No contamination of silica has been detected, as inferred by EDX analysis reported in Table S6.

2.3. Bacterial strains and growth conditions

S. aureus and *E. coli* were routinely grown at 37 °C on blood agar plates while *A. veronii* and *L. garvieae* were inoculated onto Tryptic Soy Agar supplemented with 1.5% NaCl at 25 °C. Fresh colonies were used in the experiments.

2.4. In vitro determination of the antibacterial activity

The lignin–metal oxides hybrids were assessed *in vitro* against the four bacterial strains. The activity was determined using a liquid dilution method following the CLSI protocol (Clinical and Laboratory Standards Institute), and the resulting samples were analyzed through a colony-forming unit (CFU) assay. Specifically, bacterial suspensions were prepared in phosphate-buffered saline at a concentration of 10^8 CFU/mL, and subsequently diluted 1:200 in Mueller–Hinton (MH) broth. The lignin–metal oxide samples were resuspended in MH broth at 100 mg/mL, and two-fold serial dilutions were prepared in MH broth keeping the suspension homogeneous between dilutions. For each test, 500 μL of sample was combined with 500 μL of bacterial suspension in a 24-well plate. The compounds were tested over a concentration range of 50–1.56 mg/mL. Reference ZnO and Cu_2O samples were evaluated at concentrations up to 0.25 mg/mL. Positive controls (growth medium with bacteria without addition of samples), and sterility controls (growth medium without inoculum and samples) were included. Plates were incubated at 37 °C, and after 24 h of incubation, stirred for a few minutes; 50 μL of each dilution was plated in Standard Count Agar (SCA) and incubated at 37 °C for an additional 24 h to allow colony growth from viable bacterial cells. The minimum bactericidal concentration (MBC) was defined as the lowest concentration showing no bacterial growth or fewer than ten colonies. All assays were performed in at least two independent replicates.

3. Results and discussion

This work shows the development of efficient and eco-friendly methods for producing lignin-based antimicrobial hybrid materials containing nanoparticle metal oxides. In particular, different combinations of a Kraft lignin (HMW) with a single oxide phase (ZnO or Cu_2O) or a mixture of the two has been pursued, affording materials of type HMW@ZnO, HMW@Cu_2O and HMW@ZnO_Cu_2O. In our previous studies, we demonstrated that Cu-containing materials exhibit effective *in vivo* antimicrobial properties against phytopathogens, whereas Zn-containing materials act as growth promoters in tomato plants (Vescovi et al., 2025; Gazzurelli et al., 2022, 2020). These promising results underscore the need for a more sustainable and cost-effective synthetic approach, a challenge that a mechano-assisted approach may address.

3.1. HMW@ZnO_X% materials

At first, we searched for a simple, sustainable and scalable synthesis of HMW@ZnO materials. The effectiveness of a mechanochemical transformation depends on many experimental variables. Beside reagents ratio and the amount of solvent eventually added, the duration and intensity of the milling treatment are other crucial variables. The syntheses were carried out using a planetary ball mill equipped with agate or zirconia jars (see Experimental Section for details). Stainless steel jars were avoided to prevent possible contamination by undesired metals. Different lignin/Zn^{2+}/NaOH ratios were tested using zinc salts with different counteranions ($Zn(OAc)_2·2H_2O$, $ZnCl_2$, or $ZnSO_4·7H_2O$) to evaluate possible anion effects on the growth of the ZnO NPs, since their size and morphology are known to affect antimicrobial properties (Babayevska et al., 2022). NaOH was added as a water solution to achieve LAG conditions (η values ranging from 0.7 to 1.7). The optimized conditions that led to a smooth recovery of the target products consider a brief and gentle pre-mixing of the zinc salt with HMW, followed by the addition of a NaOH water solution. The mixing was then prolonged for 30 min at 300 rpm and the product, once removed from the jar, dried at 95 °C. After washing with water, the product was dried again at the same temperature. The nature of the formed crystalline phase was verified by means of PXRD, while the amount of metal uploaded was determined by ICP-AES analysis. We selected two different target percentages, corresponding to nominal metal concentration of 5% and 10%. Full conversion of the reagents was observed using a $Zn^{2+}/OH^- = 5$ and $Zn^{2+}/OH^- = 4$ molar ratios, respectively, as evidenced by PXRD analysis. The different amount of base required for the two different materials is likely due to the higher concentration of acidic phenolic groups that feature the material containing the lowest amount of metal. ICP-AES characterization data were in good agreement with the expected percentages, returning values of 4.7 ± 0.2% (HMW@ZnO_5%) and 13.1 ± 0.1% (HMW@ZnO_13%), respectively. The diffractograms of the two materials are equivalent, with peaks corresponding to zincite (peaks at 31.8°, 34.4°, 36.3°, 47.5°, 56.7°, 62.8°, 64.4°, 67.9°, 68.3°), as can be inferred from Fig. 1A.

The use of different zinc sources did not affect the nature of the final product in terms of crystalline phase (Figure S1). FT-IR spectra of HMW@ZnO_13% and HMW are shown in Fig. 1B. The typical Kraft

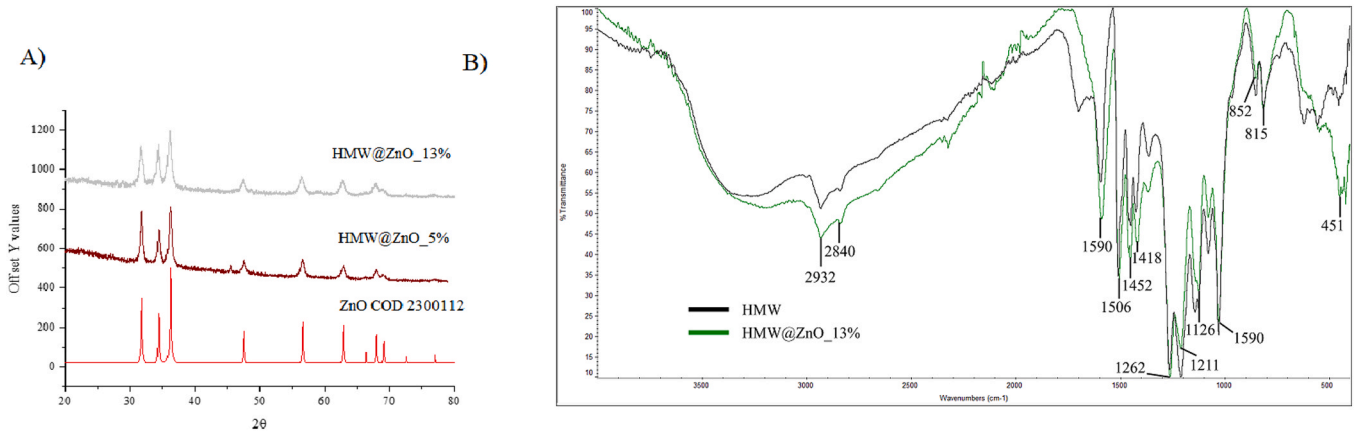


Fig. 1. A) Stacked PXRD patterns of reference ZnO (COD, code number 2300112), HMW@ZnO_5%, HMW@ZnO_13% synthesized from $ZnSO_4 \cdot 7H_2O$. B) Superimposition of FT-IR spectra of HMW@ZnO_13% (green line) and HMW (black line).

lignin signals are well visible (Boeriu et al., 2004). These include a broad band around 3400 cm^{-1} corresponding to the stretching of the hydroxyl groups, weaker bands at 2936–2835 cm^{-1} relative to the stretching of the aromatic and aliphatic C-H bonds, and a band at 1595 cm^{-1} corresponding to the stretching of the aromatic C=C bonds. The bands at 1512 and 1427 cm^{-1} correspond to the aromatic ring vibrations, while the signals at 1214 cm^{-1} and 1120 cm^{-1} are related to C-C and C-O stretches. Finally, the band at 1081 cm^{-1} confirms the presence of secondary alcohols and aliphatic ethers.

The band around 451 cm^{-1} is attributed to Zn–O stretching vibrations (Sharma and Sharma, 2023), whereas the other signals expected for ZnO are masked by bands originated by lignin. In the hybrid materials, the lignin-related bands remain almost unchanged, suggesting that the embedding of ZnO nanoparticles does not affect significantly the structure of the biopolymer.

The effect of reagent ratios on the size and morphology of the metal NPs was investigated by TEM microscopy (Fig. 2). The materials contain distinct crystalline aggregates rather than isolated structures, characterized by clustered crystalline domains. The analysis of HMW@ZnO_5% showed the presence of aggregates with dimensions of 20–200 nm constituted by elements of 10–50 nm with the sporadic presence of needles with length of 50–100 nm and thickness of 20–50 nm (Fig. 2a). The analysis of HMW@ZnO_13% revealed the presence of crystals with dimensions of 20–100 nm and the presence of needles with length of 50 nm and thickness of 5–20 nm (Fig. 2b). EDX spectra (Figure S2) and SAED analysis (Figure S3) further confirmed the nature of the oxide phase.

DLS analysis of an aqueous suspension of HMW@ZnO_5% and HMW@ZnO_13% returned the profile depicted in Figure S4 and S20. The average diameter of the particles is about 204 nm for HMW@ZnO_5% and about 139 nm for HMW@ZnO_13% (Table S5).

Given the mild milling conditions, extensive degradation of lignin chains is unlikely. However, to verify this assumption, HMW was ground under conditions similar to those applied for the synthesis of the hybrid materials, yielding HMW_g, which was subsequently characterized by FT-IR, TGA, DSC, and Py-GC-MS. As expected, the FT-IR spectra of HMW and HMW_g were superimposable (Figure S5), indicating no detectable variation in functional group distribution. The small differences observed in the thermal profiles (Figures S6 and S7) may arise from milling-induced changes in supramolecular interactions governing polymer chains packing and/or from particle size reduction, rather than from structural changes in the polymer chains. Moreover, the Py-GC-MS profiles of pristine and milled lignin showed comparable relative distributions of lignin-derived pyrolysis products (Figure S8), suggesting

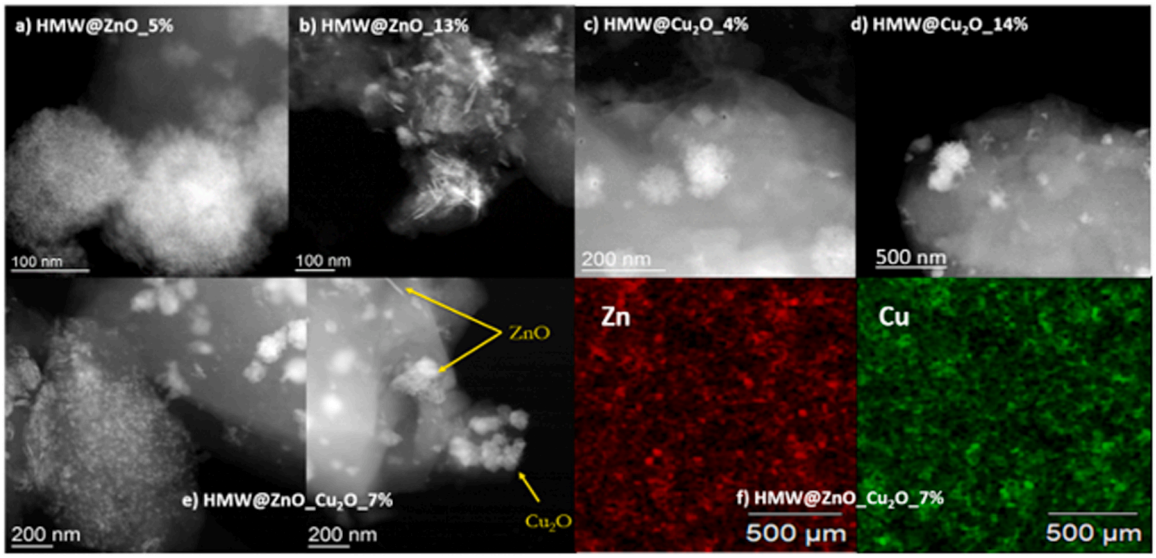


Fig. 2. TEM images of the ZnO and Cu_2O nanocrystals in HMW@ZnO_X% (a and b), HMW@Cu_2O_Y% (c and d) and HMW@ZnO_Cu_2O_7% (e) materials, highlighting the different morphologies found for the two oxides; f) elemental mapping (Zn–red, Cu–green) in HMW@ZnO_Cu_2O_7%.

that mild milling did not induce detectable chemical changes in the lignin structure. Finally, SEC analyses of HMW and HMW_g were highly comparable (Table S4), demonstrating that grinding under these conditions did not affect significantly the molecular weight distribution of the polymer. The TGA and DSC profiles of HMW@ZnO_13% (Figures S9 and S10) are similar to those previously observed for HMW@ZnO_10%, which was synthesized *via* a wet procedure (Vescovi et al., 2025). The slight differences compared with pristine HMW can be attributed to the influence of ZnO NPs on the thermal events. The Py-GC-MS profile shows a relative decrease in phenol and cresol derivatives and a concomitant increase in guaiacol, suggesting that ZnO NPs affect the pyrolytic fragmentation pathway of lignin, in agreement with previous findings (Vescovi et al., 2025).

To demonstrate the productivity of the optimized process beyond initial screening, we successfully scaled the reaction up to a 60 g batch, maintaining full conversion (Procedure S1 and Table S2), irrespective to the metal source and metal content (Figures S12 and S13).

3.2. HMW@Cu_2O_Y% materials

The preparation of HMW@Cu_2O_Y% was performed similarly to that of the Zn-containing materials (see the Experimental Section for details). After washing, the products were characterized by FT-IR, PXRD, ICP-AES, DLS, TEM and EDX analysis. ICP-AES analysis returned weight percentages of copper of 3.9% (HMW@Cu_2O_4%) and 14.3% (HMW@Cu_2O_14%), in good agreement with the expected values. The diffractograms of the two materials contain only the peaks of cuprite (29.5°, 36.42°, 42.3°, 61.36 °, 73.5° and 77.3°), as can be seen in Fig. 3A.

Fig. 3B reports overimposed FT-IR spectra of pure HMW and HMW@Cu_2O_14%. The main difference is related to the appearance, in the spectrum of the hybrid material, of the broad band in the range 500–615 cm^{-1} corresponding to Cu-O stretching, (Chang, 1992) pointing out the presence of the inorganic oxide.

TEM analysis (Fig. 2c) revealed the coexistence of spherical NPs with dimensions of 5–50 nm that tend to aggregate forming larger spherical particles having a diameter of about 100 nm. Energy dispersive X-ray spectroscopy (EDX) confirmed the presence of copper and oxygen with a ratio close to 2 (Figure S14).

DLS analysis of an aqueous suspension of HMW@Cu_2O_X% returned the profile depicted in Figure S15 and S16. As for the hybrid materials containing zincite, also in presence of cuprite a narrow size distribution of the nanoparticles was achieved, which is consistent with the polydispersity index reported in Table S5.

3.3. HMW@ZnO_Cu_2O_7% materials

Given the previously outlined advantages deriving from hybrid materials incorporating zinc oxide and cuprous oxide, (Salah et al., 2017; Hassan et al., 2017; Fen et al., 2025; Li et al., 2022) we became interested to isolate a material containing both phases to investigate possible antimicrobial synergistic effects. The experimental conditions applied for its synthesis were very similar to those used for the preparation of the monometallic materials (see Experimental for details). The synthesis was targeted on the isolation of a material containing about 10% in weight of both metals. The ICP-AES characterization returned a percentage of metal loading corresponding to 7% for both metal (7.10% and 7.35% for Zn and Cu, respectively), then the material was labelled as HMW@ZnO_Cu_2O_7%. The exclusive formation of zincite and cuprite was confirmed by PXRD analysis (Fig. 4A).

As expected, the FT-IR spectra of HMW@ZnO_Cu_2O_7% were superimposable with those of HMW@Cu_2O and HMW@ZnO (Fig. 4B). TEM analysis (Fig. 2e) revealed the presence of ZnO nanocrystals with dimensions of 10–50 nm, whose morphology could not be definitively established, and of spheres with diameter of 5–20 nm. Aggregates of 100 nm dimensions constituted by 10–20 nm elements of cuprite are also present. EDX analysis evidenced a homogeneous distribution of the two metals in the biopolymer (Fig. 2f), with very similar relative amounts of copper and zinc (Table S6). Again, DLS analysis indicates a quite broad size distribution of the nanoparticles (Figure S18 and Table S5).

3.4. Comparison between mechano-assisted and wet procedure

We have already reported the synthesis of HMW@ZnO and HMW@Cu_2O materials through wet procedures, using exclusively water as solvent and achieving metal loadings comparable to those of the materials reported in this work (Vescovi et al., 2025; Gazzurelli et al., 2022). The development of effective mechanochemical procedures is therefore not primarily justified by environmental considerations, but rather by the practical advantages offered by mechano-assisted synthesis, which avoids tedious filtration of large volumes of aqueous slurries, thereby enabling easier and faster product recovery. The advantages of mechano-assisted procedures appear particularly evident in the synthesis of HMW@Cu_2O materials, Gazzurelli et al. (2022) whose wet synthesis requires strict control of pH and copper concentration. In fact, pH values lower than 11 lead to the formation of basic sulfates, such as brochantite, $Cu_4(OH)_6(SO_4)$, and posnjakite, $Cu_4(OH)_6(SO_4)\cdot H_2O$, while copper contents higher than 4% (w/w) result in mixtures of cuprite and posnjakite. Moreover, due to the high alkalinity of the solution, the reaction must be carried out under an inert atmosphere to

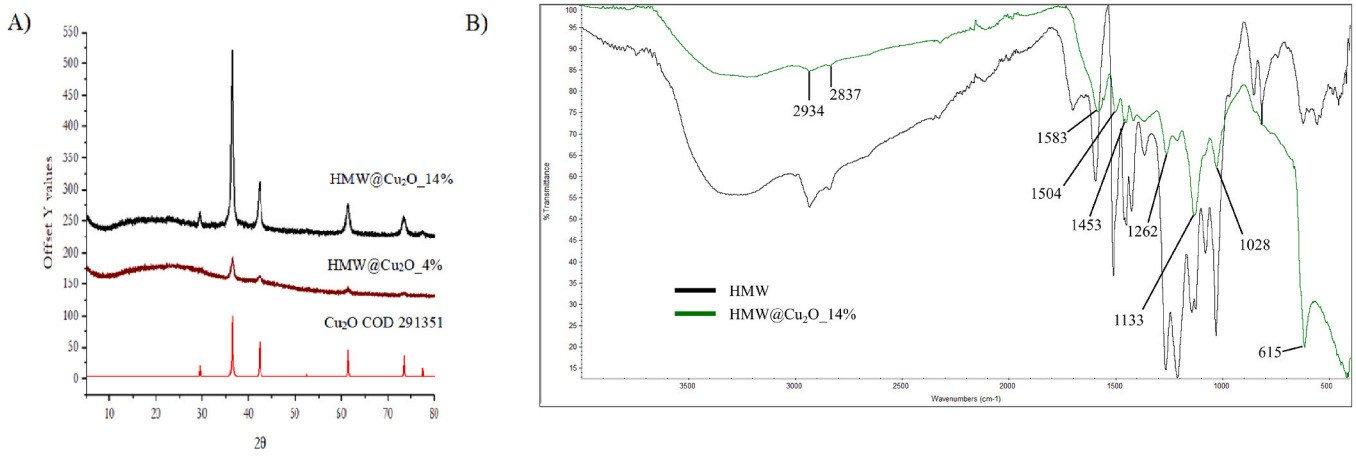


Fig. 3. A) Stacked PXRD patterns of HMW@Cu_2O_4%, HMW@Cu_2O_14% and Cu_2O (COD 291351) B) FT-IR of HMW@Cu_2O_14% (green line) and HMW (black line).

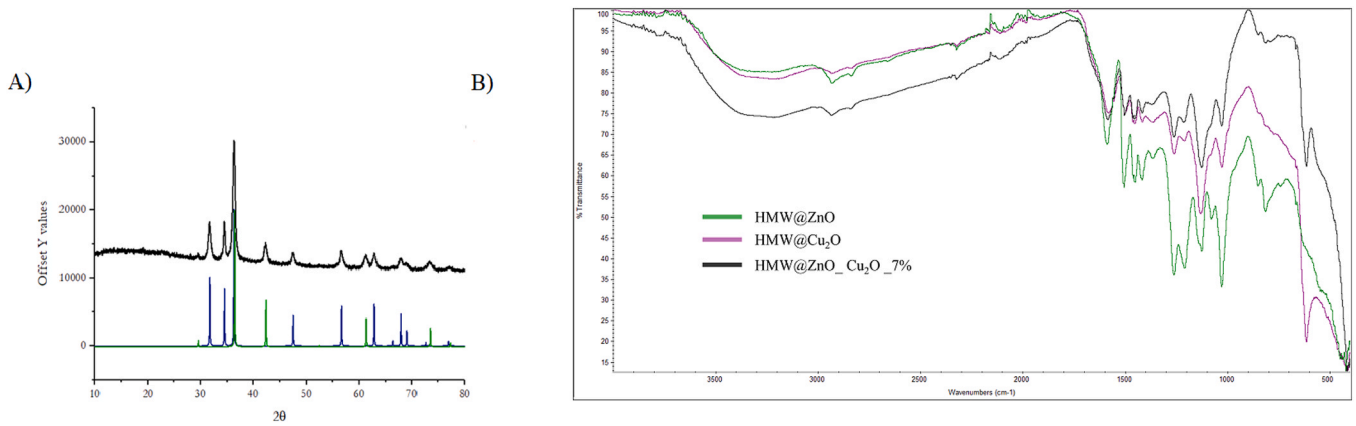


Fig. 4. A) The matching of experimental PXRD patterns of HMW@ZnO_Cu_2O 7% with Cu_2O (COD 291351, green line) and ZnO (COD 2300112, blue line). B) Superimposed FT-IR spectra of HMW@ZnO (green line), HMW@Cu_2O (violet line) HMW@ZnO_Cu_2O (black line).

avoid the formation of significant amounts of sodium carbonate. In contrast, high selectivity towards cuprite was observed under mechanochemical conditions, with the straightforward isolation of materials loaded with different copper percentages, without the need of an inert atmosphere. From the comparison of the characterization data, it follows that the wet and mechanochemical materials are rather similar (Figure S21 and Table S5). In fact, in case of low ZnO loading (HMW@ZnO_5%, Table S5, entries 1 and 2) the mechanochemical product contains NPs with a diameter of 10–50 nm and thickness of 5–20 nm, forming aggregates of 20–200 nm, and a DLS distribution centered at 204.4 nm. In the corresponding wet material, the NPs have smaller diameters (10–20 nm) and similar thickness (10–20 nm), but slightly larger aggregates of 20–300 nm are found, with a DLS profile centered at 137 nm. With higher ZnO loadings (Table S5, entries 3 and 4), the diameter (20–100 nm compared with 10–20 nm) and thickness (5–20 nm compared with 10–50 nm) are lower in the mechanochemical product, but NPs aggregation is more evident in the wet material, as reflected in the DLS profiles (139 nm compared with 156 nm, respectively). For HMW@Cu_2O materials, the comparison is possible only for the materials corresponding to 4% copper loading (Table S5, entries 5 and 6), since with higher loadings the wet procedure leads to the formation of phases different from cuprite. A single population of NPs having a diameter of 5–20 nm forms under mechanochemical conditions, forming aggregates of about 100 nm. The wet procedure leads instead to two different NP populations, with diameter of 100 nm and 200 nm. The DLS profiles have maxima at 194 nm and 184 nm, respectively.

3.5. Antibacterial activity

Due to the intrinsic color and limited solubility of the lignin-based hybrid materials, microbiological assays were conducted by incubating the samples in a liquid medium, followed by transfer of the resulting suspensions onto solid agar plates to assess bacterial regrowth (Fig. 5). Thus, the method allowed to identify the minimum bactericidal concentration (MBC) that is defined as the lowest concentration at

Table 2
MBC (mg/mL) obtained for the tested compounds. Values represent the range of concentrations at which no bacterial regrowth was observed after subculture on agar plates.

	MBC values (mg/mL)			
	S. aureus	*L. garvieae*	*E. coli*	*A. veronii*
HMW	> 50	> 50	> 50	50
HMW@ZnO_13%	50–25	50	> 50	25–12.5
HMW@Cu_2O_14%	25	25–12.5	25	12.5–6.25
HMW@ZnO_Cu_2O_7%	12.5	25–12.5	25	6.25–3.125
ZnO	8	8	8	> 8
Cu_2O	4	4	4	4

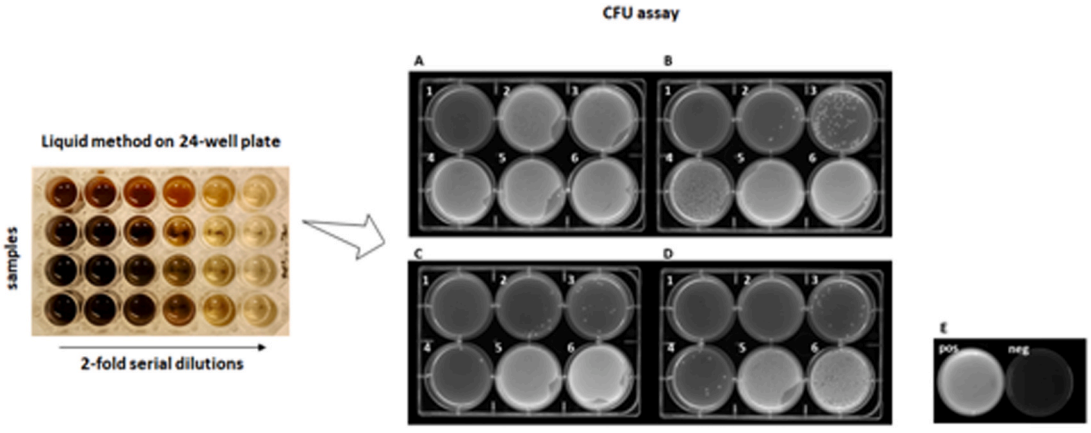


Fig. 5. Illustration of the experimental workflow: 500 μL of sample and 500 μL of bacterial suspension are incubated at 37 °C for 24 h, then 50 μL of each dilution is plated on agar plates and incubated at 37 °C for additional 24 h. On the right, representative images of CFU assay of *A. veronii* following a 24h-incubation at the different experimental conditions are reported. (A) HMW, (B) HMW@ZnO, (C) HMW@Cu_2O, (D) HMW@ZnO_Cu_2O, (E) control samples. 1–6: serial 2-fold dilutions in the range 50–1.56 mg/mL. The minimum bactericidal concentration (MBC) is defined as the lowest concentration showing no bacterial growth or a number of colonies fewer than ten.

which no bacterial growth was observed on the agar plates, indicating complete loss of bacterial viability under the tested conditions (Table 2). Lignin-based materials were assayed over a concentration range of 50–1.56 mg/mL, whereas ZnO and Cu_2O reference samples were evaluated at concentrations ranging from 8 to 0.25 mg/mL, corresponding to the metal oxide content loaded onto the hybrid materials as determined by ICP-AES.

The results indicate that all metal oxide hybrid materials exhibited bactericidal activity against the tested strains compared to lignin matrix, except for *E. coli*, which remained resistant even at the highest tested concentration of HMW@ZnO (MBC > 50 mg/mL). The MBC values varied depending on both bacterial species and the material composition; when comparing the single oxide hybrid materials, HMW@Cu_2O was consistently the most effective formulation, with MBC values reduced by one to two two-fold dilution steps compared to HMW@ZnO, confirming the higher antimicrobial potency of copper-based systems compared to zinc-based ones. This trend is in agreement with the MBC values obtained for Cu_2O and ZnO reference samples which were 4 mg/mL and 8 mg/mL, respectively, across all tested bacterial strains.

Notably, the dual-metal system HMW@ZnO_Cu_2O exhibited the lowest MBC value against *S. aureus* and *A. veronii*, despite containing a reduced total loading of metal oxides compared to the single-metal systems. In these representative Gram-positive and Gram-negative bacterial models, the enhanced performance of the dual-metal system suggests a positive interaction between ZnO and Cu_2O, whereby their co-presence promotes complementary antimicrobial mechanisms beyond what would be expected from a simple additive contribution of the individual components. Based on the ZnO and Cu_2O contents in the tested samples, in fact, the hybrid materials achieved MBC values at a significantly lower metal oxide content than pure zincite and cuprite. Specifically, HMW@ZnO_Cu_2O, containing 0.55 mg/mL of ZnO and 0.52 mg/mL of Cu_2O, displayed MBC value of 6.25 mg/mL for *A. veronii*; at these metal concentrations, the reference pure samples did not exhibit bactericidal activity since their MBC values are > 8 mg/mL for ZnO and 4 mg/mL for Cu_2O (Figure S22). Overall, it can be stated that the simultaneous presence of both metal oxides intensifies their well-documented mechanism of activity, such as intracellular oxidative stress and membrane damage, increasing the potency of the lignin-based hybrid materials.

Albeit preliminary, the antibacterial assays demonstrated that embedding metal oxides within a lignin matrix can lower the metal oxide content required to achieve a robust bactericidal effect. However, further studies are needed to elucidate the underlying mechanism of action, particularly regarding potential synergistic effects.

4. Conclusions

This study has demonstrated the feasibility of using a mechano-assisted approach for the synthesis of hybrid materials combining lignin with metal oxide nanoparticles, leading to the smooth formation of products containing well-defined amounts of Zn, Cu or both metals. The advantages offered by mechano-assisted over solution-based procedures come mainly from the easy recovery of the final products, avoiding tedious filtration or centrifugation steps. The materials obtained were fully characterized by means of several techniques, including FT-IR, XRPD, TEM, ICP-AES, DLS, TGA; DSC, Pyrolysis GC-MS. Small metal-oxide NPs with sizes in the range 5–50 nm were found, forming larger aggregates up to 300 nm, which are however smaller than those found with the materials prepared under wet procedures. DLS analyses evidenced a narrow size distribution of the nanoparticles, with PDIs in the range 0.09–0.28 nm. Preliminary assessment of the antibacterial activity of the HMW@ZnO, HMW@Cu_2O and HMW@ZnO_Cu_2O materials returned very promising results. Comparing single-oxide materials, HMW@Cu_2O was the most potent, particularly against the Gram-negative strain *A. veronii*. Crucially, the hybrid integrating both metal oxides (HMW@ZnO_Cu_2O_7%) showed superior efficacy against *S. aureus* and *A. veronii*, exhibiting lower MBC values than the highest concentration single-oxide materials (HMW@ZnO_13% and HMW@Cu_2O_14%). Given the lower total metal content in the hetero-metallic hybrid, these results strongly suggest a cooperative effect mechanism where the combination of oxides enhances the overall bactericidal performance. Importantly, based on the ZnO and Cu_2O contents in the tested samples, the hybrid materials achieved MBC values at a significantly lower metal oxide content (up to 9 or 37 times lower in *A. veronii*) than pure zincite and cuprite. This effect may arise from the complementary antimicrobial mechanisms of the two oxides. ZnO is known to contribute to bacterial inactivation primarily through the generation of reactive oxygen species (ROS) and the release of Zn^{2+} ions, which can disrupt membrane integrity and interfere with enzymatic activity. In parallel, Cu_2O can exert strong bactericidal effects via Cu^{+}/Cu^{2+} ion release, inducing oxidative stress, lipid peroxidation, and protein dysfunction.

Finally, all hybrid materials showed enhanced antibacterial activity compared to the corresponding ZnO and Cu_2O reference samples, thereby validating the effectiveness of the mechanochemical synthesis approach for developing potent, lignin-based metal oxide antimicrobials. However, cytotoxicity and biocompatibility evaluations were not performed in this study and will be addressed in future work, with assays to be designed in view of potential applications in human health and aquatic environmental contexts, in order to fully assess their safety profile.

Supporting information

The Supporting Information is available free of charge at https://pubs.acs.org/doi/xxx (PDF file). Procedure description for scale up synthesis of HMW@ZnO_X% materials (Procedure S1). Stoichiometric ratios for the preparation of the materials (Tables S1-S2). Operating parameters for ICP analysis (Table S3). SEC analysis (Table S4). Comparison between mechano-assisted and wet synthesis (Table S5). EDX and SAED analyses (Table S6, Figures S2, S3, S14, S17). DLS analyses (Figures S4, S15, S16, S18, S20). PXRD patterns (Figures S1, S12, S19). IR spectra (Figures S5, S19). TGA and DSC analyses (Figures S6, S7, S9, S10). Pyrolysis GC/MS (Figures S8, S11).

CRediT authorship contribution statement

Marianna Vescovi: Writing – original draft, Investigation, Formal analysis, Data curation. **Diego Pini:** Formal analysis, Data curation. **Andrea Gustinelli:** Writing – review & editing, Formal analysis. **Giorgia Bignami:** Writing – review & editing, Formal analysis. **Andrea Migliori:** Writing – original draft, Investigation, Data curation. **Lisa Menegaldo:** Writing – original draft, Investigation, Formal analysis, Data curation. **Francesca Bonvicini:** Writing – original draft, Investigation, Formal analysis, Data curation. **Dominga Rogolino:** Writing – original draft, Supervision, Investigation, Funding acquisition, Formal analysis, Data curation, Conceptualization. **Paolo Pelagatti:** Writing – original draft, Supervision, Investigation, Funding acquisition, Data curation, Conceptualization.

Funding

DP PhD-scholarship was funded by Regione Emilia Romagna PR FSE+ 2021/2027 (progetti di formazione per la ricerca 40° e 41° ciclo. Territorio: Transizione tecnologica, culturale, economica e sociale verso la sostenibilità).

Declaration of Competing Interest

The authors declare that they have no known competing financial interests or personal relationships that could have appeared to influence the work reported in this paper.

Acknowledgment

The authors thank Dr. Monica Maffini for technical support. This work has benefited from the equipment and framework of the COMP-HUB Initiative, funded by the 'Departments of Excellence' program of the Italian Ministry for Education, University and Research (MIUR, 2018–2022 and MUR, 2023–2027).

Appendix A. Supporting information

Supplementary data associated with this article can be found in the online version at doi:10.1016/j.indcrop.2026.124404.

Data availability

Data will be made available on request.

References

Abebe, B., Zereffa, E.A., Tadesse, A., Murthy, H.C.A., 2020. A review on enhancing the antibacterial activity of ZnO: mechanisms and microscopic investigation. Nanoscale Res. Lett. 15 (1), 190. https://doi.org/10.1186/s11671-020-03418-6.

Ao, W., Li, J., Yang, H., Zeng, X., Ma, X., 2006. Mechanochemical synthesis of zinc oxide nanocrystalline. Powder Technol. 168, 148–151. https://doi.org/10.1016/j.powtec.2006.07.014.

Babayevska, Przysiecka, N., Iatsunskyi, I., et al., 2022. ZnO size and shape effect on antibacterial activity and cytotoxicity profile. Sci. Rep. 12, 8148. https://doi.org/10.1038/s41598-022-12134-3.

Beisl, S., Friedl, A., Miltner, A., 2017. Lignin from Micro- To Nanosize: Applications. Int. J. Mol. Sci. 18, 2367.

Boeriu, C.G., Bravo, D., Gosselink, R.J.A., van Dam, J.E.G., 2004. Characterisation of structure-dependent functional properties of lignin with infrared spectroscopy. Ind. Crops Prod. 20 (2), 205–218. https://doi.org/10.1016/j.indcrop.2004.04.022.

Boldyrev, V.V., Tkáčová, K., 2000. Mechanochemistry of Solids: Past, Present, and Prospects. J. Mater. Synth. Process. 8, 121–132. https://doi.org/10.1023/A:1011347706721.

Chang, A., 1992. Fourier Transform Infrared (FTIR) Analysis of Copper Oxide Thin Films Prepared by Metal Organic Chemical Vapor Deposition (MOCVD). MRS Online Proc. Libr. 293, 443. https://doi.org/10.1557/PROC-293-443.

Chetry, A.B., 2025. Mechanochemistry: A new frontier in chemical synthesis. J. Chem. Res. 49 (3), 17475198251339299. https://doi.org/10.1177/17475198251339299.

Dong, X., Dong, M., Lu, Y., Turley, A., Jin, T., Wu, C., 2011. Antimicrobial and Antioxidant Activities of Lignin from Residue of Corn Stover to Ethanol Production. Ind. Crops Prod. 34, 1629–1634.

Esposito, G., Bignami, G., Colussi, S., Pastorino, P., Bondavalli, F., Fioravanti, M.L., Bozzetta, E., Acutis, P., Valentino, A., Rizzi, R., Gustinelli, A., Prearo, M., 2025. Expanding Horizons: The First Reported Outbreak of Piscine Lactococcosis in Farmed Gilthead Seabream *Sparus aurata* in the Northern Tyrrhenian Sea. J. Fish. Dis. 48 (7), e14121. https://doi.org/10.1111/jfd.14121.

Fen, Y., Xinxin, M., Yang, X., Jianjian, D., Dan, D., Xinyan, C., Rui, D., Xiaolei, W., 2025. Engineered hollow Cu_2O@ZnO p-n heterojunction nanocomposites for synergistic photocatalytic disinfection and tissue regeneration. J. Mater. Chem. B 13 (38), 12246–12256. https://doi.org/10.1039/d5tb01635e.

Gazzurelli, C., Carcelli, M., Mazzeo, PP., Mucchino, C, Pandolfi, A., Migliori, A., Pietarinen, S., Leonardi, G., Rogolino, D., Pelagatti, P., 2022. Exploiting the Reducing Properties of Lignin for the Development of an Effective Lignin@Cu_2O Pesticide. Adv. Sustain. Syst. 6 (8), 2200108. https://doi.org/10.1002/adsu.202200108.

Gazzurelli, C., Migliori, A., Mazzeo, P.P., Carcelli, M., Pietarinen, S., Leonardi, G., Pandolfi, A., Rogolino, D., Pelagatti, P., 2020. Making Agriculture More Sustainable: An Environmentally Friendly Approach to the Synthesis of Lignin@Cu Pesticides. ACS Sustain. Chem. Eng. 8 (39), 14886–14895. https://doi.org/10.1021/acssuschemeng.0c04645.

Hassan, I.A., Sathasivam, S., Nair, S.P., Carmalt, C.J., 2017. Antimicrobial Properties of Copper-Doped ZnO Coatings under Darkness and White Light Illumination. ACS Omega 2 (8), 4556–4562. https://doi.org/10.1021/acsomega.7b00759.

Huang, Z., Feng, P., Wu, X., et al., 2026. Green synthesis of aminated lignin via biocatalytic pathway for removal of Cu(II) from wastewater. AIChE J. 72 (6), e70320. https://doi.org/10.1002/aic.70320.

Jacukowicz-Sobala, I., Kociołek-Balawejder, E., Stanisławska, E., Seniuk, A., Paluch, E., Wiglusz, R.J., Dworniczek, E., 2023. Biocidal activity of multifunctional cuprite-doped anion exchanger – Influence of bacteria type and medium composition. Sci. Total. Environ. 891, 164667. https://doi.org/10.1016/j.scitotenv.2023.164667.

James, S.L., Adams, C.J., Bolm, C., Braga, D., Collier, P., Friščić, T., Grepioni, F., Harris, K.D.M., Hyett, G., Jones, W., Krebs, A., Mack, J., Maini, L., Orpen, A.G., Parkin, I.P., Shearouse, W.C., Steed, J.W., Waddell, D.C., 2012. Mechanochemistry: opportunities for new and cleaner synthesis. Chem. Soc. Rev. 41 (1), 413–447. https://doi.org/10.1039/c1cs15171a.

Karmanova, A.P., Ermakova, A.V., Raskoshaa, O.V., Bashlykovaa, L.A., Rachkovaa, N.G., Kocheva, L.S., 2021. Structure and Biomedical Properties of Lignins (A Review). J. Appl. Spectrosc. 88, 182–192.

Khayati, G.R., Nourafkan, E., Karimi, G., Moradgholi, J., 2013. Synthesis of cuprous oxide nanoparticles by mechanochemical oxidation of copper in high planetary energy ball mill. Adv. Powder Technol. 24 (1), 301–305. https://doi.org/10.1016/j.apt.2012.07.006.

Klapiszewska, I., Parus, A., Ławniczak, Ł., Jesionowski, T., Klapiszewski, Ł., Ślosarczyk, 2021. A. Production of antibacterial cement composites containing ZnO/lignin and ZnO–SiO_2/lignin hybrid admixtures. Cem. Concr. Compos. 124, 104250. https://doi.org/10.1016/j.cemconcomp.2021.104250.

Lejeune, B.T., Zhang, X., Sun, S., Hines, J., Jinn, K.W., Reilly, A.N., Clark, H.A., Lewis, L. H., 2023. Enhancing Biocidal Capability in Cuprite Coatings. ACS Biomater. Sci. Eng. 9 (7), 4178–4186. https://doi.org/10.1021/acsbiomaterials.2c01222.

Li, M., Chen, Z., Yang, L., Li, J., Xu, J., Chen, C., Wu, Q., Yang, M., Liu, T., 2022. Antibacterial Activity and Mechanism of GO/Cu_2O/ZnO Coating on Ultrafine Glass Fiber. Nanomaterials 12, 1857. https://doi.org/10.3390/nano12111857.

Lu, X., Gu, X., Shi, Y., 2022. A review on lignin antioxidants: Their sources, isolations, antioxidant activities and various applications. Int. J. Biol. Macromol. 210, 716–741. https://doi.org/10.1016/j.ijbiomac.2022.04.228.

Meghana, S., Kabra, P., Chakraborty, S., Padmavathy, N., 2015. Understanding the pathway of antibacterial activity of copper oxide nanoparticles. RSC Adv. 5, 12293–12299. https://doi.org/10.1039/C5RA01312G.

Radhika, N.L., Sachdeva, S., Kumar, M., 2022. Lignin depolymerization and biotransformation to industrially important chemicals/biofuels. Fuel 312, 122935. https://doi.org/10.1016/j.fuel.2021.122935.

Salah, N., Habib, S.S., Khan, Z.H., Memic, A., Azam, A., Alarfaj, E., Zahed, N., Al-Hamedi, S., 2017. High-energy ball milling technique for ZnO nanoparticles as antibacterial material. J. Nanomater., 1637362 https://doi.org/10.1155/2017/1637362.

Salogni, C., Bertasio, C., Accini, A., Gibelli, L.R., Pigoli, C., Susini, F., Podavini, E., Scali, F., Varisco, G., Alborali, G.L., 2024. The Characterisation of Lactococcus garvieae Isolated in an Outbreak of Septicaemic Disease in Farmed Seabass (Dicentrarchus labrax, Linnaues 1758) in Italy. Pathogens 13, 49. https://doi.org/10.3390/pathogens13010049.

Sharma, D.K., Shukla, S., Sharma, K.K., Kumar, V., 2022. A review on ZnO: Fundamental properties and applications. Mater. Today. Proc. 49, 3028–3035. https://doi.org/10.1016/j.matpr.2020.10.238.

Sharma, P., Sharma, N., 2023. Lignin Derived from Forestry Biomass as Capping Reagent in the Biosynthesis and Characterization of Zinc Oxide Nanoparticles and Their In Vitro Efficacy as a Strong Antifungal Biocontrolling Agent for Commercial Crops. BioNanoSci 13, 36–48. https://doi.org/10.1007/s12668-022-01052-3.

Tothova, E., Senna, M., Yermakov, A., Kovac, J., Dutkova, E., Hegedüs, M., Kanuchova, M., Baláz, M., Lukacova, Z., Bujnakova, J., Briancin, P., Makreski, P., 2020. Zn source-dependent magnetic properties of undoped ZnO nanoparticles from mechanochemically derived hydrozincite. J. Mater. Chem. C. 8, 9075–9085. https://doi.org/10.1039/D0TC02045E.

Tsuzuki, T., 2009. Commercial scale production of inorganic nanoparticles. Int. J. Nanotechnol. 6, 567–578. https://doi.org/10.1504/IJNT.2009.027457.

Tsuzuki, T., 2021. Mechanochemical synthesis of metal oxide nanoparticles. Commun. Chem. 4, 143. https://doi.org/10.1038/s42004-021-00582-3.

Vasile, C., Baican, M., 2023. Lignins as Promising Renewable Biopolymers and Bioactive Compounds for High-Performance Materials. Polymers 15, 3177. https://doi.org/10.3390/polym15153177.

Verdini, F., Gaudino, E.C., Canova, E., Tabasso, S., Behbahani, P.J., Cravotto, G., 2022. Lignin as a Natural Carrier for the Efficient Delivery of Bioactive Compounds: From Waste to Health. Molecules 27 (11), 3598. https://doi.org/10.3390/molecules27113598.

Vescovi, M., Maffini, M., Pietarinen, S., Leonardi, G., Migliori, A., Woo, S., Manganiello, G., Lanzuise, S., Michelino, M., Careri, M., Pelagatti, P., Rogolino, D., 2025. Sustainable Lignin@ZnO Hybrid Materials: Synthesis, Characterization, and Preliminary Biostimulant Assessment in Tomato Plants. Adv. Sustain. Syst. 9 (10), e00399. https://doi.org/10.1002/adsu.202500399.

Vescovi, M., Melegari, M., Gazzurelli, C., Maffini, M., Mucchino, C., Mazzeo, P., Carcelli, M., Perego, J., Migliori, A., Leonardi, G., Pietarinen, S., Pelagatti, P., Rogolino, D., 2023. Industrial lignins as efficient biosorbents for Cr(VI) water remediation: transforming a waste into an added value material, 1709–1717 RSC Sustain. 1, 1423–1435. https://doi.org/10.1039/D3SU00081H.

Wang, Y., Lu, Z., Liu, B., Seidi, F., Zhang, C., Jiang, B., Huang, C., Xiao, H., Wang, P., Jin, Y., 2024. Antitumor Effects of Carrier-Free Functionalized Lignin Materials on Human Hepatocellular Carcinoma (HepG2) Cells. ACS Nano 18 (5), 4329–4342. https://doi.org/10.1021/acsnano.3c09924.

Wang, Y., Zhou, S., Zhuang, Z., An, X., Wu, W., Jiang, B., Zhang, C., Manan, S., Wang, P., Jin, Y., 2025. Lignin-Based Therapeutics: Targeting Mitochondrial Pathways in Osteosarcoma. J. Agric. Food Chem. 25 73 (25), 15967–15980. https://doi.org/10.1021/acs.jafc.5c01065.

Wenger, L.E., Hanusa, T.P., 2023. Synthesis without solvent: consequences for mechanochemical reactivity. Chem. Commun. 59, 14210–14222. https://doi.org/10.1039/D3CC04929A.

World Health Organization, 2014. Antimicrobial resistance: global report on surveillance. WHO.

World Health Organization, 2022. WHO. *GLASS report 2022* (.

Yu, X., Yang, B., Zhu, W., Deng, T., Pu, Y., Ragauskas, A., Wang, H., 2023. Towards functionalized lignin and its derivatives for high-value material applications. Ind. Crops Prod. 200 (Part A), 116824. https://doi.org/10.1016/j.indcrop.2023.116824.

Zrnčić, S., 2020. Diagnostic Manual for the main pathogens in European seabass and Gilthead seabream aquaculture. Zaragoza: CIHEAM, 172 p. (Options Méditerranéennes: Série B). Etudes Et. Rech. 75. http://om.ciheam.org/om/pdf/b75/b75.pdf (n).